

See discussions, stats, and author profiles for this publication at: <https://www.researchgate.net/publication/231666508>

# Raman Investigation of Uncoated and Coated Magnetic Fluids

ARTICLE *in* THE JOURNAL OF PHYSICAL CHEMISTRY A · MARCH 2000

Impact Factor: 2.69 · DOI: 10.1021/jp9937306

---

CITATIONS

28

---

READS

11

4 AUTHORS, INCLUDING:



P. C. Morais

University of Brasília

437 PUBLICATIONS 4,498 CITATIONS

SEE PROFILE



Sebastião W da Silva

University of Brasília

103 PUBLICATIONS 967 CITATIONS

SEE PROFILE

## Raman Investigation of Uncoated and Coated Magnetic Fluids

Paulo Cesar Morais,<sup>†,\*</sup> Sebastião William da Silva,<sup>†</sup> Maria Aparecida Godoy Soler,<sup>†</sup> and Norbert Buske<sup>‡</sup>

Universidade de Brasília, Instituto de Física, Núcleo de Física Aplicada C.P. 04455, CEP 70919–970 Brasília-DF, Brazil, and Mediport Kardiotechnik GmbH, Wiesenweg 10, D-12247 Berlin, Germany

Received: October 19, 1999; In Final Form: January 7, 2000

We report on room-temperature Raman spectra of OH stretching modes associated to the surface of uncoated, single-coated, and double-coated nanomagnetic particles in hydrocarbon and water-based magnetic fluids. The data are compared with liquid water and discussed in terms of the suppression of symmetric and asymmetric hydrogen bonded modes. The hydrogen bond strength associated to the hydroxyl-group in the uncoated nanomagnetic particle is enhanced by 14% with respect to liquid water. In contrast, in the double-coated nanomagnetic particle the hydrogen bond strength is reduced by 13% with respect to liquid water. Within the sensitivity of our experimental setup, however, no indication of hydrogen bond was found in the case of the single-coated nanomagnetic particle. Finally, in the single-coated sample the hydroxyl grafting coefficient is reduced by a factor of 3.2 with respect to the double-coated sample.

### 1. Introduction

Magnetic fluids (MF) are stable colloids consisting of monodomain nanomagnetic particles dispersed in organic<sup>1</sup> or inorganic<sup>2</sup> solvents. Such a unique material system encompasses the properties of both liquids and solids, thus accounting for the great interest on its fundamental properties and practical applications. The recent effort toward production of biocompatible<sup>3</sup> MF is justified once expectations around a variety of applications have been raised, as for instance, in drug delivery systems<sup>4</sup> and contrast agents in magnetic resonance imaging.<sup>5</sup> As far as the biomedical applications are concerned, the physicochemical properties of the molecular layer chemisorbed at the nanoparticle surface plays a key role. Despite of that, little has been done to investigate the structure and the interaction of the molecular layer bonded at the nanoparticle surface with the surrounding medium. In drug delivery systems, for instance, one seeks to achieve the highest biological specificity associated to the ideal grafting coefficient. The biological specificity and the grafting coefficient of a bioactive molecule depend on the efficiency of the link between the molecule and the nanoparticle surface. However, before the nanoparticle can be coated with a particular drug species at a given grafting coefficient, its surface has to be molecular designed using precoating molecules. Among the experimental techniques used to investigate MF neither the traditional birefringence measurements<sup>6</sup> nor the unconventional magnetic resonance of doped samples<sup>7</sup> would be of great help to monitor the molecular layer chemisorbed at the nanoparticle surface. In contrast, Raman spectroscopy has been very recently introduced to investigate MF, and is a promising and powerful technique to probe the chemical species chemisorbed at the

nanoparticle surface in both aspects, structure and interaction with the surface as well as with surrounding medium.<sup>8</sup> In the present work, we extend the use of the Raman spectroscopy to investigate the nanoparticle surface material in water-based and hydrocarbon-based MF. In particular, the usefulness of the Raman spectroscopy to track the degree of grafting of precoating species linked to the surface of nanomagnetite-based particles is demonstrated. The Raman probe used to investigate the grafting coefficient is the OH stretching mode (around 3500 cm<sup>-1</sup>) associated to the hydroxyl group, which is chemisorbed at the nanoparticle surface since the very beginning of its chemical synthesis.

### 2. Experimental Section

The samples used in the present work were obtained by chemical coprecipitation of Fe(II) and Fe(III) ions in alkaline medium, following peptization in different solvents, as described elsewhere.<sup>9</sup> Transmission electron microscopy was used to obtain the average nanoparticle diameter (8 nm) and the corresponding logarithmic standard deviation (0.26). Molecular-uncoated Fe<sub>2</sub>O<sub>3</sub> nanoparticle as well as molecular-coated Fe<sub>3</sub>O<sub>4</sub> nanoparticle were peptized as stable MF containing  $2.5 \times 10^{16}$  particle/cm<sup>3</sup>. The uncoated MF sample (Fe<sub>2</sub>O<sub>3</sub>) was peptized in aqueous acid medium. The two coated MF samples (Fe<sub>3</sub>O<sub>4</sub>) were peptized in hydrocarbon and water medium. In the single-coated MF the Fe<sub>3</sub>O<sub>4</sub> nanoparticle was treated with dodecanoic acid and peptized in hydrocarbon. In the double-coated MF the Fe<sub>3</sub>O<sub>4</sub> nanoparticle was first coated with dodecanoic acid, following treatment with an ethoxylated polyalcohol and finally peptized in water. The Raman setup consists of a double 0.85 m 1401 Spex monochromator equipped with the usual photo-counting system, featured with a dark count of 5 s<sup>-1</sup>. The samples were optically excited with the 514 nm line from an argon ion laser, at an optical power on the order of 150 mW, outside the sample holder. The laser beam passes vertically through the sample holder, i.e., parallel to the spectrometer entrance slit. The scattered light is collected from a small

\* Corresponding author: Universidade de Brasília, Instituto de Física, Núcleo de Física Aplicada, C. P. 04455, CEP 70919-970 Brasília (DF), Brazil. E-mail: pcmor@fis.unb.br. Fax/Phone: (+55) 61-2723151/61-2736655.

<sup>†</sup> Universidade de Brasília.

<sup>‡</sup> Mediport Kardiotechnik GmbH.

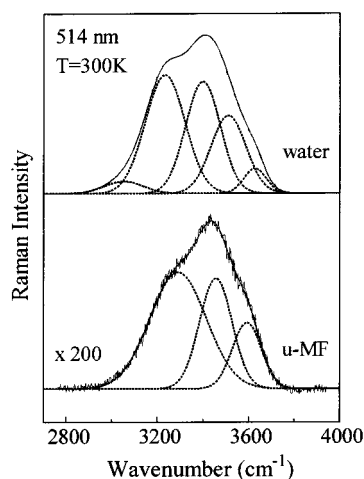


**Figure 1.** Raman spectra in the OH stretching region of liquid water (upper frame) and u-MF (lower frame). The solid lines represent the best fit using Gaussian-shaped components. Dotted lines represent the deconvoluted Raman modes.

rectangular area of about  $\frac{1}{2}$  mm wide  $\times$  1 mm high. The Raman measurements were performed at room temperature in the typical range of the intramolecular OH stretching modes (around  $3500\text{ cm}^{-1}$ ).

### 3. Results and Discussion

The Raman spectra of aqueous-based systems are dominated by the OH stretching modes occurring in the range of  $3000\text{--}4000\text{ cm}^{-1}$  and arising from the various amounts of hydrogen bonding. Usually, the Raman data are analyzed within the framework of a tetrahedral bonded structure.<sup>10</sup> The two OH stretching Raman components at the higher end frequency of the spectra describe non-hydrogen bonded modes ( $\nu^s$  and  $\nu^a$ ). In contrast, the four Raman components at lower frequencies describe hydrogen bonded modes ( $\nu_d^s$ ,  $\nu_d^a$ ,  $\nu_b$  and  $\nu_w$ ).<sup>10,11</sup> However, it has been shown that the Raman intensity of the  $\nu_w$  mode is very low compared to the other OH stretching modes and thus only five modes instead of six are used to fit the experimental data in liquid water.<sup>11</sup> Figure 1 shows the room temperature Raman spectra of both the liquid water and the uncoated magnetic fluid sample (u-MF), in the OH stretching mode region. Figure 2 shows the room temperature Raman spectra of the double-coated (d-MF) and single-coated (s-MF) magnetic fluid samples. In Figures 1 and 2 the solid lines represent the best fit of the experimental data using Gaussian-shaped components. The dotted lines in Figures 1 and 2, however, represent each Raman mode individually, according to our fitting procedure. Table 1 presents the main parameters resulting from the best fit of the Raman spectra. In Table 1 the full width at half-maximum intensity (FWHM) associated to the Raman lines of water and u-MF are given in parentheses. The spectrum taken from the u-MF sample shows the presence of only three OH stretching modes, thus confirming the suppression of the two symmetric OH stretching modes in comparison with liquid water.<sup>8</sup> The presence of only three Raman modes associated to the u-MF, in the OH stretching region, is supported by a simple calculation using the classical approximation. This is a strong evidence that the Raman spectrum of the u-MF, in the  $3000\text{ cm}^{-1}$  to  $4000\text{ cm}^{-1}$  range, is dominated by the hydroxyl-group chemisorbed at the nanoparticle surface. The presence of such a hydroxyl-based layer around nanometer-sized particles dispersed in water-based colloids plays a key role on the colloidal stability and on many

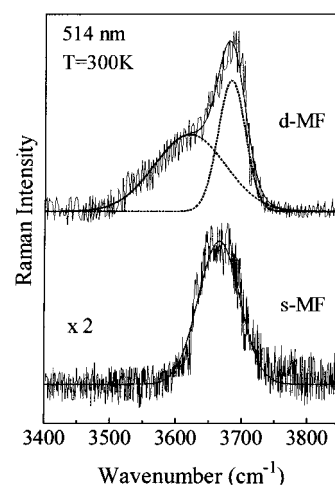


**Figure 2.** Raman spectra in the OH stretching region of the d-MF (upper frame) and s-MF (lower frame). The solid lines represent the best fit using Gaussian-shaped components. Dotted lines represent the deconvoluted Raman modes.

**TABLE 1: OH Stretching Raman Modes of Liquid Water, u-MF, d-MF, and s-MF, at Room Temperature and Ambient Pressure**

sample	Raman modes ( $\text{cm}^{-1}$ )					$\Delta H$ (kcal/mol)
	$\nu_d^s$	$\nu_d^a$	$\nu_b$	$\nu^s$	$\nu^a$	
Water	3051 (85)	3233 (87)	3399 (76)	3511 (76)	3628 (49)	2.74
u-MF		3291 (123)	3457 (71)		3593 (63)	3.13
d-MF			3620		3683	2.38
s-MF					3663	

<sup>a</sup> The correspondent hydrogen bond strength values ( $\Delta H$ ) are quoted in the last column. The FWHM are quoted in parenthesis, in units of  $\text{cm}^{-1}$ .

of their very optical properties, as recently demonstrated.<sup>12</sup> Magnetic resonance measurements have been used to estimate the thickness (about 1.1 nm) of the hydroxyl-based layer around the nanomagnetic particles in ionic magnetic fluids.<sup>13</sup> The presence of only three Raman modes ( $\nu_d^a$ ,  $\nu_b$ , and  $\nu^a$ ) in the u-MF, in comparison to the five Raman modes observed in liquid water, is a consequence of the vibrational quenching effect due to the replacement of a hydrogen atom from the water molecule by the nanomagnetic particle surface, as discussed elsewhere.<sup>8</sup> Note from Table 1 that the FWHM associated to the  $\nu_d^a$  Raman mode is abnormally high in the u-MF sample in comparison to the water. In addition, the  $\nu_d^a$  Raman mode is wider in the uncoated  $\text{Fe}_2\text{O}_3$  nanoparticles compared to the uncoated  $\text{CuFe}_2\text{O}_4$  and  $\text{ZnFe}_2\text{O}_4$  nanoparticles as well.<sup>8</sup> In fact the understanding of this anomaly needs further investigation. Further, from the data obtained in this work, it is found that the  $\nu_d^a$  Raman mode is suppressed from the spectrum obtained with the d-MF sample. In addition, both  $\nu_d^a$  and  $\nu_b$  Raman modes are suppressed from the spectrum obtained with the s-MF sample. The understanding of the quenching of the  $\nu_d^a$  Raman mode from both d-MF and s-MF samples is straightforward once the dodecanoic layer, which is chemisorbed at the nanoparticle surface, inhibits water molecules from the medium to bond to the OH-groups at the nanoparticle surface. The quenching of an extra Raman mode ( $\nu_b$ ) from the s-MF sample, however, is mainly attributed to the lack of a hydrogen bond between the residual OH-group chemisorbed at the nanoparticle surface and either the long carbon chain from the dodecanoic acid or from the solvent. Therefore, the only Raman mode left behind in the

hydrocarbon-based s-MF is the asymmetric non-hydrogen bonded one ( $\nu^a$ ). Note that the possibility of a hydrogen bond between the residual OH-group chemisorbed at the nanoparticle surface and the OH-group from the ethoxylated polyalcohol accounts for the presence of the  $\nu_b$  Raman mode in the d-MF. Further, the remarkable intensity reduction of the OH stretching Raman lines in the d-MF and s-MF samples as compared to the u-MF sample is a clear indication of the water grafting reduction, due to the chemisorption of the dodecanoic acid. Besides, the area ratio taken from the Raman OH stretching modes in the d-MF sample with respect to the s-MF sample is on the order of 3.2, reflecting the surface grafting ratio associated to the OH-group. Such a remarkable surface grafting reduction (a factor of 3.2), when one goes from the d-MF toward the s-MF, would be due to a combination of two factors. First, the hydrogen bond between the OH-group from the nanoparticle surface and the OH-group from the ethoxylated polyalcohol in the d-MF may help to maintain a higher hydroxyl grafting coefficient. Second, the effect of the solvent itself in the d-MF, i.e., the aqueous medium would favor a higher hydroxyl grafting coefficient as well. A quantitative description of these issues, however, requires further experimental and theoretical investigations.

The data in Table 1 show a wavenumber upshift of the Raman stretching modes in the coated MF with respect to the uncoated MF. In qualitative grounds the wavenumber upshift reflects a weaker interaction between the OH-group from the nanoparticle surface and the coating layer. The significant wavenumber upshift of the  $\nu_b$  Raman mode in the d-MF ( $163\text{ cm}^{-1}$ ) with respect to the u-MF, supports the picture of a weaker hydrogen bond established between the OH-group chemisorbed at the nanoparticle surface and the second coating layer (ethoxylated polyalcohol). In contrast, the wavenumber upshift of the  $\nu^a$  Raman mode in the d-MF ( $90\text{ cm}^{-1}$ ) with respect to the u-MF, is about half of that observed in the case of the  $\nu_b$  Raman mode. Note that the hydrogen bonded Raman modes indicate more efficiently the interaction established between the OH-group chemisorbed at the nanoparticle surface and the surrounding medium. A quantitative analysis of the hydrogen bond strength or the enthalpy change ( $\Delta H$ ) can be performed using the van't Hoff equation.<sup>14</sup> The approximate calculation is based on the liquid water equilibrium ( $\text{O}-\text{H}\cdots\text{O} \rightleftharpoons \text{O}-\text{H} + \text{O}$ ), to which is assigned an enthalpy of  $\Delta H = 2.53\text{ kcal/mol}$ .<sup>11</sup> The liquid water equilibrium constant ( $K$ ) is related to the ratio  $A_B/A_U$ .  $A_B$  is the sum of the integrated Gaussian Raman components related to the hydrogen bonded OH stretching modes.  $A_U$  is the sum of the integrated Gaussian Raman components related to the non-hydrogen bonded OH stretching modes. The van't Hoff equation reads  $\ln K = A - \Delta H/RT$ , where  $R = 1.99\text{ cal/mol K}$  is the gas constant,  $T$  is the absolute temperature, and  $A = -3.579$  is the intercept constant for liquid water.<sup>11</sup> Though approximate, we assume the intercept constant for the MF samples equals to  $-3.579$ . So, the hydrogen bond strength can be estimate from the Raman data, as shown in the last column of Table 1. The enthalpy change we found for liquid water ( $\Delta H = 2.74\text{ kcal/mol}$ ) is in very good agreement with the literature. The enthalpy change of the u-MF is enhanced by about 14% with respect to the value found for liquid water, in good agreement with previous results.<sup>8</sup> However, the enthalpy change of the d-MF

is reduced by about 13% with respect to the value found in liquid water, in accordance with the discussion above concerning the wavenumber upshift. Finally, as the s-MF presents no Raman line associated to the  $\nu_b$  mode the enthalpy change should be taken as zero. This is an approximation, meaning that the Raman signal associated to the  $\nu_b$  mode in the s-MF is below the sensitivity of the experimental setup (dark count of  $5\text{ s}^{-1}$ ).

#### 4. Conclusions

In conclusion, Raman spectroscopy has been successfully used to investigate the relative degree of grafting of a particular coating agent, using the OH-group to probe the nanoparticle surface in s-MF and d-MF. In the u-MF, three Raman OH stretching modes have been observed in accordance with previous work.<sup>8</sup> In contrast, in the double-coated  $\text{Fe}_3\text{O}_4$  MF two Raman OH stretching modes have been observed, while in the single-coated  $\text{Fe}_3\text{O}_4$  MF only one Raman OH stretching mode has been observed. The suppression of the  $\nu_d^a$  Raman mode from the d-MF and s-MF is assumed to be due to the lack of hydrogen bond between the OH-group at the nanoparticle surface and the molecules in the medium. Steric hindering due to the first coating layer may prevent the water molecule from the medium to approach the nanoparticle surface. Suppression of an extra Raman mode ( $\nu_b$ ) from the s-MF spectrum is assumed to be due the absence of hydrogen bonding involving the OH-group chemisorbed at the nanoparticle surface. Reduction of the spectra area ratio associated to the OH stretching modes in the s-MF with respect to the d-MF suggests a decrease of the hydroxyl surface grafting by a factor of 3.2. Finally, the wavenumber upshift observed in the coated MF as compared to the uncoated MF goes parallel with the reduction on the enthalpy change ( $\Delta H$ ) associated to the hydrogen bonding involving the OH-group.

**Acknowledgment.** This work was partially supported by the Brazilian agencies FAP-DF, CAPES, and CNPq.

#### References and Notes

- (1) Khalafalla, S. E.; Reimers, G. W. U.S. Patent 3764540, 1973.
- (2) Massart, R. U.S. Patent 4329241, 1982.
- (3) Lacava, Z. G. M.; Azevedo, R. B.; Lacava, L. M.; Martins, E. V.; Garcia, V. A. P.; Rebola, C. A.; Lemos, A. P. C.; Sousa, M. H.; Tourinho, F. A.; Morais, P. C.; Da Silva, M. F. *J. Magn. Magn. Mater.* **1999**, *194*, 90.
- (4) Lacava, Z. G. M.; Martins, E. V.; Freitas, M. L. L.; Coelho, E. M. S.; Sousa, M. H.; Da Silva, M. F.; Azevedo, R. B.; Tourinho, F. A.; Morais, P. C. *J. Magn. Magn. Mater.* **1999**, *201*, 431.
- (5) Kuznetsov, A. A.; Filippov, V. I.; Kuznetsov, O. A.; Gerlivanov, V. G.; Dobrinsky, E. K.; Malashin, S. I. *J. Magn. Magn. Mater.* **1999**, *194*, 22.
- (6) Jung, C. W.; Rogers, J. M.; Groman, E. V. *J. Magn. Magn. Mater.* **1999**, *194*, 185.
- (7) Socoliuc, V.; Rasa, M.; Sofonea, V.; Bica, D.; Osvath, L.; Luca, D. *J. Magn. Magn. Mater.* **1999**, *191*, 241.
- (8) Silva, G. J.; Morais, P. C.; Tourinho, F. A. *J. Phys. Chem.* **1996**, *100*, 14269.
- (9) Morais, P. C.; da Silva, S. W.; Soler, M. A. G.; Sousa, M. H.; Tourinho, F. A. *J. Magn. Magn. Mater.* **1999**, *201*, 105.
- (10) Günther, D.; Buske, N. D.E. Patent 4325386, 1993.
- (11) Scherer, J. R.; Go, M. K.; Kint, S. J. *J. Phys. Chem.* **1974**, *78*, 1304.
- (12) Carey, D. M.; Korenowski, G. M. *J. Chem. Phys.* **1998**, *108*, 2669.
- (13) Qu, F.; Morais, P. C. *J. Chem. Phys.* **1999**, *111*, 8588.
- (14) Morais, P. C.; Tourinho, F. A.; Gonçalves, G. R. R.; Tronconi, A. L. *J. Magn. Magn. Mater.* **1995**, *149*, 19.
- (15) Walrafen, G. E.; Fisher, M. R.; Hokmabadi, M. S.; Yang, W.-H. *J. Chem. Phys.* **1986**, *85*, 6970.